Published in final edited form as:
J Magn Reson Imaging. 2012 February ; 35(2): 309–317. doi:10.1002/jmri.22835.

Comprehensive Brain Analysis with Automated High Resolution Magnetization Transfer Measurements

Ying Wu, MD[a,b,*], **Hongyan Du, MS**[c], **Pippa Storey, PhD**[d], **Christopher Glielmi, PhD**[e], **Fiona Malone**[a,f], **Shawn Sidharthan, BS**[a], **Ann Ragin, PhD**[g], **Paul S. Tofts, PhD**[h], and **Robert R. Edelman, MD**[a]

[a]Radiology, NorthShore University HealthSystem; 2650 Ridge Ave, Walgreen G555. Evanston IL, 60201

[b]Radiology, University of Chicago; 5841 S. Maryland Avenue, Chicago, IL 60637

[c]Center for Clinical Research Informatics, NorthShore University HealthSystem; 2650 Ridge ave, Evanston IL, 60201

[d]Radiology New York University; 550 First Avenue, New York, NY 10016

[e]Siemens Healthcare, MR Research and Development; Chicago, IL

[f]University of Chicago; 5801 South Ellis Avenue, Chicago, Illinois 60637

[g]Radiology, Northwestern University; Northwestern Radiology, 737 North St. Clair Street, Suite 1600, Chicago, Illinois 60611-2927

[h]Brighton and Sussex Medical School, Falmer, Sussex BN1 9PX, UK

Abstract

Purpose—This investigation aimed to enhance the reliability and spatial resolution of MTR measurements for interrogation of subcortical brain regions with an automated volume of interest (VOI) approach.

Materials and Methods—A 3D MT sequence was acquired using a scan-rescan imaging protocol in 9 healthy volunteers. VOI definition masks for the MTR measurements were generated using FreeSurfer and compared to a manual region of interest (ROI) approach. (The longitudinal stability of MTR was monitored using agar gel phantom over a 5-month period.) Intra-class correlation coefficients (ICC), coefficients of variation (CV) and instrumental standard deviation (ISD) were determined.

Results—CVs ranged from1.29–2.64% (automated) vs. 1.30–3.40% (manual). ISDs ranged from 0.62–1.10 pu (automated) vs. 0.68–1.67 pu (manual). The SD of the running difference was 1.70% for the phantom scans. Bland-Altman method indicated interchangeability of the automated VOI and manual ROI measurements.

Conclusions—The automated VOI approach for MTR measurement yielded higher ICCs, lower CVs and lower ISDs compared to the manual method, supporting the utility of this strategy. These

[*]Corresponding Author: Ying Wu MD., Director of Image Processing Lab, Office: 847-5701118, Lab: 847-5704279, Fax: 847-5702942, YWu@northshore.org.

results demonstrate the feasibility of obtaining reliable MTR measurements in hippocampus and other critical subcortical regions.

Keywords

magnetization transfer imaging; magnetization transfer ratio; 3T; segmentation; volume of interest; reproducibility

INTRODUCTION

Pathological changes in the brain can occur many years prior to the appearance of clinical symptoms in Alzheimer's disease (AD), Parkinson's disease (PD), and multiple sclerosis (MS). For example, lesions may develop in the hippocampus ten years prior to the clinical onset of AD (1,2). About 70% of nigra cells have been lost in the substantia nigra when the clinical symptoms of PD present (3). Alterations in the brain are detected as early as eight years before the presentation of disabilities associated with MS (4). Neuroimaging techniques that can adequately assess the small brain regions vulnerable to early impairment could reduce the long observation periods in current clinical practice. Reliable and reproducible neuroimaging tools are requisite for conducting longitudinal evaluations in the small brain regions that are critical to an understanding of natural history and for assessing the effectiveness of treatment.

The Magnetization Transfer Ratio (MTR), which is calculated based on the signal intensity difference with and without MT saturation can detect subtle brain abnormalities that are not apparent with conventional MR techniques (5, 6, 7). Post-mortem studies have shown that decreased MTR is associated disrupted micro structural integrity of myelin macromolecules. MTR has been studied extensively in white matter in MS. The physiologic significance and clinical relevance of MTR in gray matter is not as well understood. However, abnormalities have been identified with MTR in both white and gray matter (8–10). These findings have contributed to our knowledge of MTR and underlying pathology. Pathologically, astrocytic hyperplasia, patchy oedema, perivascular infiltration, myelin thinning and axonal loss have been shown in white matter structures (11–12), while diffuse demyelination (13), axonal transection and apoptotic loss of neurons (14) have been among findings in gray matter. In neurodegenerative diseases such as AD and PD, subtle changes occurring in gray matter may be critical for early detection. MT has shown clinical utility in neurodegenerative disorders such as AD, PD, HIV-Dementia, as well as in psychiatric disorders (15–30).

The majority of clinical applications using MT have been performed at 1.5T (31–35). Although, MT at 3T has not been widely used in clinical settings, several studies have shown that MT can be safely executed at 3T with improved image quality and enhanced signal to noise ratio (SNR) (36–39). Application of MT for *in vivo* measurement of small brain structures is hindered by several technical limitations. Typically, thick slices (e.g. 3–5 mm) have been prescribed with prolonged scan times to cover the whole brain (15, 17–22). Moreover, intra- and inter-rater variation introduced by the necessity of manually outlining regions of interest (manual ROI), have not been addressed. This may result in suboptimal measurement consistency and is particularly problematic for longitudinal studies (40).

Towards this end, we further reduced the slice thickness reported in two previous 3T MT studies from 3mm to near isotropic 1.2mm covering the entire brain in less than 15 minutes (33, 36, 37, 41). This investigation determined whether optimized high resolution MT at 3T can be used to assess the hippocampus, small basal ganglia structures and deep white matter regions. Further, we addressed operator variability; manual analysis was completely eliminated by integrating a segmentation algorithm and establishing a fully automated post processing pipeline. Healthy volunteers, as well as a customized agar phantom, were used to assess MTR reproducibility using a scan-rescan approach. For comparison, both automated and manual measurements were obtained.

MATERIALS AND METHODS

Image acquisition

Whole brain images of nine healthy subjects (6 males, 3 females, mean age: 33 yrs.; range: 18–65) were obtained using a 12-channel multi-array receive coil used with body-coil transmission on a 3 Tesla system (MAGNETOM Verio, Siemens Healthcare, Erlangen, Germany, VB15b) (35). The MR protocol included a 3-plane localizer, 3D MP-RAGE and 3D high resolution MT acquired at two different time points in all subjects. The interval between the repeated scans was approximately one week. For the anatomic T1-weighted MP-RAGE, the Alzheimer's Disease Neuroimaging Initiative (ADNI) standard protocol (42) was used with the following parameters: TR=2300 ms, TE=2.94 ms, TI=900 ms, flip angle 9°, 160 slices scanned for sagittal plane with 1.2 mm slice thickness and the scanning matrix was 256 × 256 with a field of view of 256 mm, resulting in a voxel size of 1.0 × 1.0 × 1.2 mm^3. Total scan time was 9:14. To account for possible head tilting, the scan plane for MP-RAGE was angled according to the mid-line on the axial and coronal images of the brain on the 3-plane localizer.

The high resolution MT acquisition was a 3D MT-weighted fast spoiled gradient echo (GRE) pulse sequence with the following parameters: TR=30 ms, TE=4 ms, flip angle 10°, 96 1.2 mm slices scanned for sagittal plane and the scanning matrix was 256 × 256 with a field of view of 256 mm, resulting in a voxel size of 1.0 × 1.0 × 1.2 mm^3. Receiver bandwidth was 200 Hz/Pixel and an 81.3% rectangular field of view was used to reduce the scan time without compromising the resolution. Given the focus on small brain structures, efforts were made to accelerate the scan for whole brain coverage with thinner slices. Partial Fourier acquisition was applied in both phase encoding and slice-encoding directions resulting in scan time of 6:35. To avoid more extensive SNR degradation, parallel imaging was not used. For each scan, the MT sequence was run twice, once preceded by an off-resonant saturation pulse ($\mathbf{M_S}$) and once without the saturation pulse ($\mathbf{M_0}$). MT preparation included a Gaussian shape saturation pulse at 1200 Hz offset from water resonance with duration of 10 ms (FWHM = 4.5 ms) and flip angle of 500°. Care was taken to keep the receiver gain constant throughout the M_S and M_0 acquisitions.

A single comparison dataset at 1.5T (MAGNETOM Avanto, Siemens Healthcare, Erlangen, Germany) was obtained for visual assessment. Scan parameters and post-processing protocols were identical except for the MT saturation default values which were 1500 Hz offset from water resonance with duration of 7.7 ms (FWHM = 3.5 ms). Identical pre-

scanning settings (e.g. center frequency, shim parameters, transmit gain, and receiver gains) were maintained between the MS and M0 acquisitions. These parameters were optimized based on a published 3D SPGR model previously (36, 43). Careful AC-PC localization for the high resolution MT scans was used to minimize inter-scan variation from head positioning at the two time-points. SAR was maintained below FDA limits using the system's hardware monitor to ensure patient safety. The study was approved by the Institutional Review Board and informed consent was provided by all subjects.

Image analysis

Quantitative image analysis was performed off-line. MR images were transferred to a Linux workstation and the 3D high resolution MTR maps were calculated for the whole brain pixel-by-pixel. The analysis was performed using customized image processing software written using FSLUTILS (FSL, FMRIB, Oxford, UK) (Smith et al., 2004). Maps of the MTR were computed using the relation, $MTR=\frac{M_0-M_s}{M_0}$ where M_S and M_0 are the signal intensities in a given voxel obtained with and without the MT saturation pulse. MTR is expressed as percentage units (pu). The whole brain MTR maps for the second time-point were spatially aligned to the baseline maps using FLIRT (FSL, FMRIB, Oxford, UK) (44).

MTR measurements—The automated method and the conventional manual method were obtained for further comparison.

Automated Volume of Interest (VOI) Measurements: Using the T1-weighted MP-RAGE images of time point 1, automated masks of brain regions were generated using FreeSurfer (Martinos Center for Biomedical Imaging, Massachusetts General Hospital, Harvard Medical School, MA) (45). MTR maps of both timepoints were spatially aligned to the automated masks through co-registration to derive volumes of interest as follows: 1) the transformation matrix was first computed by aligning each time point M_0 to the normalized T1-weighted image, a FreeSurfer derived interim image set that possesses the same orientation of the structural mask by FreeSurfer. 2) The transformation matrix produced from step 1 then was applied to align the MTR map of each timepoint to the structural mask generated from timepoint 1(43). Alignment was accomplished using FLIRT (FSL, FMRIB, Oxford, UK). 3) The 3D MTR volumes were extracted for various brain regions. 4) For each brain region, morphological erosion was applied at the border of the 3D MTR volume to minimize partial volume effects from neighboring tissue and to address inevitable alignment errors. MeanMTR was computed and defined as the average MTR of all voxels in the 3D volume of interest. Various registration algorithms were tested and a mutual information algorithm was chosen for conducting spatial alignment. No manual interaction was required for the automated VOIs. All procedures were fully automatic for deriving the automated VOI MTR measurements for gray matter regions, hippocampus (Hipp), Amygdala (Amyg), caudate (Cau), putamen (Put), thalamus (Thal), and white matter volumes of interest: Anterior corpus callosum (Genu), posterior corpus callosum (Splen) and left white matter (WM) and right WM. The average VOI sizes (averaged for the group) were: Genu:799 mm^3, Splen:936 mm^3; also averaged for left and right: Hipp:7670 mm^3, Amyg:3645 mm^3, Cau: 6915 mm^3, Put:11146 mm^3, Thal:13017 mm^3, WM:434795 mm^3.

Manual ROI Measurements: The MTR maps of time-point 1and 2 were spatially aligned as aforementioned above. Two separate operators independently placed ROIs (30 ~ 43mm^2) manually (46–47) on the MTR maps in specified brain gray matter regions (hippocampus (Hipp), amygdala (Amyg), caudate (Cau), putamen (Put), thalamus (Thal), subcortical white matter, Anterior corpus callosum (Genu) and posterior corpus callosum (Splen) and frontal white matter (FWM). The meanin each ROI was measured (34, 48). Each operator repeated this process so that both intra- and inter-operator variation associated with manual measurements could be determined.

Phantom Scans: To further study the reliability of MTR measurements over longer periods, an agar phantom was constructed with six tubes containing different concentrations of homogeneous agar gel (0.5%, 1%, 1.5%, 2%, 2.5%, 5%) (43). For evaluating the phantom measurements, the ROIs were positioned at the center of the tubes. MTR measurements were obtained at 17 different time-points across a period of 5 months with the following parameters: TR= 30 ms, TE=5 ms and FA=5° Receiver Bandwidth= 260 Hz/pixel. These scanning parameters were slightly different from the human study because they were matched to another ongoing MTR study. MTR measurements for the phantom images were manually performed by one operator. Mean values of MTR were calculated for each tube at each of the 17 time-points.

Statistical methods

Primary variables for analysis included the mean MTR for each subcortical region. For each separate anatomical region, mean was calculated by method (automated vs. manual), time-point (1 vs. 2), and measurement (1 vs. 2).

To validate whether the new automated VOI measurement can replace the standard manual ROI measurement, the agreement between automated and manual technique was evaluated by Bland-Altman plots in which difference between repeated measures was plotted against the average. 95% agreement limits were computed as $\bar{d} \pm 1.96s$, where $\bar{d}$ is the mean difference, and s is the standard deviation of the differences (49).

Reproducibility between MTR values at 2-time points for the manual and automated measurements was assessed using intra-class correlation coefficient (ICC) and coefficient of variation (CV), as well as the instrumental standard deviation (ISD) (50, 51). ICCs were computed through a one-way random effects ANOVA model by assuming each subject was randomly selected from a larger population of different set of two time points. The one-way ANOVA yielded a between-subject mean square (BMS) and a within-subject mean square (WMS). ICC was computed as the ratio of the subject variance (difference between BMS and WMS) and the total variance (sum of BMS and WMS) $(ICC(1,1)=\frac{BMS-WMS}{BMS+WMS})$ (52). An ICC approaching 1 would indicate high reproducibility in each case. ISD was computed to measure the instrumental variation, using Bland-Altman analysis to estimate the SD of a single measurement, and ISD is calculated as the root mean square (RMS) value of the differences divided by $1.4\,(\sqrt{\frac{\sum (x_{1i}-x_{2i})^2}{n}}/1.4)$, where n is the total number of repeated

measures, *i*=1, 2, *n*…n. (49–50, 53). The CV was estimated as the variation divided by the mean of the different time- point measurements (54).

In addition, the rater dependent variation was assessed for the manual approach using CV. Two raters each performed measurements twice on two time-point MRI scans. To calculate intra-rater variation, we randomly identified one operator and one time-point. To calculate inter-rater variation, we randomly identified one time-point and one manual measurement.

For phantom results, the instrumental variation was represented by SD of the running difference which was computed as percentage difference in signal at adjacent time points (50). All statistical tests were executed in SAS 9.2 (Cary, NC) using a significance level of $p<0.05$.

RESULTS

Fig. 1 shows examples of the near isotropic resolution MTR maps. At 3T, high tissue conspicuity was observed for brain anatomy including small regions such as the hippocampus. No loss of image quality was observed in the reformatted coronal and sagittal images. Increased tissue conspicuity and reduced noise were observed for all spatial directions (axial, sagittal, coronal) at 3T compared with 1.5T.

Fig. 2 shows examples of the automated VOI outlining using FreeSurfer brain segmentation and shows the alignment between the MT maps and the segmentation masks.

Table 1 reports the mean MTR measurements for both the automated (range 39–51 pu) and the manual ROI methods (range 40–53 pu). Fig. 3shows the validation of the automated measurements with respect to manual measurements using the Bland-Altman method in the hippocampus. This Bland-Altman plot indicated that differences in mean MTR derived from the automated method and the manual method were within 95% agreement limits in the left and right hippocampus suggesting good agreement between the two methods. Good agreement between the automated and manual derived MTR are indicated in all studied regions (data not shown).

The scan-rescan reproducibility was reported in Table 1. In general, the reproducibility of the automated method outperformed the manual method for all of the three statistical tests. 10 of 14 studied brain regions yielded ICC>0.9 for the automated method vs. 5 of 14 studied brain regions for the manual method. CV ranged from 1.29–2.64% for the automated method vs. 1.30–3.40% for the manual method. ISD ranged 0.62 to 1.10 pu for automated method vs. 0.66 to 1.67 pu for the manual method. Importantly, automated MTR measurements in the technically challenging hippocampal areas demonstrated excellent scan-rescan agreement (ICC: left=0.92 and right=0.94; CV: left=2.33% and right=1.83%; ISD: left: 0.93 pu and right=0.73 pu), while the manual ROI measurement showed considerably lower scan-rescan reproducibility (ICC: Left=0.76 and right=0.84; CV: left=4.03% and right=3.01%; ISD: left=1.67 pu and right=1.23 pu).

For intra-rater variation among different brain structures studied, CV ranged from 1.4 to 5.34%. For inter-rater variation, the CV ranged from 2.01 to 5.11% (Table 2). In the

contrast, the fully automated method avoids the operator introduced bias prevalent in manual methods.

Experimental results for the agar phantom were obtained from multiple repeated scans over 5 months. Instrumental variation evaluated by the SD of running difference was 1.7% for the 5.0% agar. For the different agar concentrations, higher agar concentrations are associated with higher MTR values and a lower running difference (Table 3).

DISCUSSION

This investigation was conducted to obtain reliable MTR measurements at 3T through automated VOI MTR analysis based on an optimized 3D MT scan with a focus in subcortical brain regions of clinical interest (43). The results indicated that the measurements derived with automated VOI method are in good agreement with those of the conventional manual ROI method. Moreover, the automated VOI method improved the scan-rescan measurement reproducibility evidenced by three different statistical assessments.

Several studies have demonstrated MT can be safely performed at 3T and with increased SNR (36, 55, 56). However, 3T has not been fully exploited for clinical applications. Compared to previous studies, the current investigation succeeded in decreasing slice thickness (1.2mm vs. 3mm) while optimizing image resolution at 3T. The availability of multi-array coil reception enabled us to gather images with excellent conspicuity in all scanning directions, and afford thinner slices. As a result improved spatial resolution is obtained in the MT scans. Typically, 3–5mm slice thickness has been used in studies of neurological diseases, i.e. in AD (15, 18, 57). With thick image slices, the MTR measurements may be influenced by partial volume averaging with neighboring tissues. Several studies have obtained thinner slices (1.5 mm) at hippocampus at 1.5T (16, 58). Higher SNR and resolution afforded by 3T is a considerable advantage for conspicuity of these small brain regions of interest. Such benefits have enhanced visibility of subthalamic nuclei for deep brain stimulus implantation and maximized tissue conspicuity for MS lesion detection (38, 59).

Manual ROI placement has generally been used when obtaining regional MTR (48, 51) for localized white matter and gray matter structures. This approach is labor intensive and subject to intra- and inter-rater variation that may result in suboptimal reproducibility (51, 60) (Fig. 4a). The chronic progressive nature of neurodegenerative diseases necessitates repeated and reliable follow-up evaluations in order to document disease development or monitor effects of therapy. We have applied a segmentation algorithm to extract regional MTR. We were able to extract MTR measurements of subcortical gray and white matter regions without operator manual input (4b). Automated regional MTR measurement in subcortical structures has not been previously reported. This investigation showed that all the automated MTR measurements for both subcortical gray and deep white matter regions are reproducible and outperformed the manual ROI convention. In all studied regions, the automated VOI measurements were consistently lower than that of the manual ROI method. The Bland-Altman results indicated that the measurements derived with automated VOI

method are in good agreement with that of the conventional manual ROI method and are interchangeable.

MTR of white matter regions has been established as a reliable index and been utilized in various multi-center clinical trials. Berry et al reported standardized MTR readouts across 7 medical centers through ROIs in frontal white matter regions. Tofts et al. used MTR of whole brain white matter as a known constant to investigate sources of variation for both scanning and post processing for multi-center studies (34, 35). Information concerning reliability of gray matter regions, however, is limited. In particular, MTR of gray matter regions are less homogeneous, therefore, requiring more technical ability to place ROIs for identical tissues over time. Manual placement of ROI's for sampling identical tissues is inherently unreliable due to the subjectivity of rater judgment and other factors such as scan repositioning at different time-points and changes in plane orientation. Advantages of the strategy proposed here for reliability may owe to the near isotropic image resolution that facilitated more accurate alignment between two images from the different time-points. In addition, the VOI approach is based on the neuro anatomical boundaries which facilitate more standardized extraction between time points, relative to manual outlining.

In comparison to the previous reports, in which MTR reproducibility of white matter regions have shown ISD range between 0.4–1pu (mean values are 30–48 pu) (35, 44, 50, 61–66) at the lower field strength of 1.5T. In this investigation, reproducibility of the automated approach for all studied brain regions, including both homogenous white matter and less homogenous subcortical grey matter regions was within this accepted range (ISD of white matter: 0.64–0.92 pu; mean value 49.23–51.31 pu; ISD of gray matter: 0.62 – 1.10 pu; mean values: 39.05–45.97). (Table 1), with ISD of large VOIs of left and right white matter (sd 0.6–0.8 pu; mean value was 49 pu). Notably, we demonstrated reliable MTR even for small brain regions, such as hippocampus, putamen, and caudate. This study supports MTR feasibility and reproducibility for neurological outcome studies in AD and other neurodegenerative diseases.

Normal control subjects provide the ultimate test of reproducibility accounting for subject dependent variations and specific tissue types. By reporting ongoing serial phantom measurements, 3T scanner stability was further assessed to monitor events such as system upgrades that occurred during the study period.

Various sources of measurement error can be introduced by inconsistencies in both acquisition and image post-analysis (35). Several scanning guidelines were strictly followed in the image acquisition (35, 37). By combining high resolution MT and automated postprocessing, high measurement consistency was achieved and improved effectively compared to the manual convention. Reliable measurements obtained free of human interaction for post processing may serve as a basis of standardization for future larger studies such as multicenter investigations.

Acknowledgments

Grant Support: This study was supported in part by the Alzheimer's Drug Discovery Foundation (ADDF) -271222; NorthShore Clinical Collaborative Research Program Award; NorthShore Pilot grant EH08-125; NorthShore Early Career Research Development Award and NIH 1R01MH080636-01A2.

We are grateful for the assistance of Nadia Abbasi and Christine O'Brien.

References

1. Braak H, Braak E. Morphology of Alzheimer disease. Fortschr Med. 1991; 108(33):621–624. [PubMed: 2289729]
2. Braak H, Braak E. Neuropathological stageing of Alzheimer-related changes. Acta Neuropathol. 1991; 82(4):239–259. [PubMed: 1759558]
3. Braak H, Ghebremedhin E, Rüb U, et al. Stages in the development of Parkinson's disease-related pathology. Cell Tissue Res. 2004; 318(1):121–134. [PubMed: 15338272]
4. Agosta F, Rovaris M, Pagani E, et al. Magnetization transfer MRI metrics predict the accumulation of disability 8 years later in patients with multiple sclerosis. Brain. 2006; 129(Pt 10):2620–2627. [PubMed: 16951409]
5. Filippi M, Rocca MA, Martino G, et al. Magnetization transfer changes in the normal appearing white matter precede the appearance of enhancing lesions in patients with multiple sclerosis. Ann Neurol. 1998; 43(6):809–814. [PubMed: 9629851]
6. Mezzapesa DM, Rocca MA, Pagani E, et al. Evidence of subtle gray-matter pathologic changes in healthy elderly individuals with nonspecific white-matter hyperintensities. Arch Neurol. 2003; 60(8):1109–1112. [PubMed: 12925367]
7. Kubicki M, Shenton ME, Salisbury DF, et al. Voxel-based morphometric analysis of gray matter in first episode schizophrenia. Neuroimage. 2002; 17(4):1711–1719. [PubMed: 12498745]
8. Agosta F, Rovaris M, et al. Magnetization transfer MRI metrics predict the accumulation of disability 8 years later in patients with multiple sclerosis. Brain. 2006; 129(Pt 10):2620–2627. [PubMed: 16951409]
9. Ge Y, Grossman RI, et al. Magnetization transfer ratio histogram analysis of normal-appearing gray matter and normal-appearing white matter in multiple sclerosis. J Comput Assist Tomogr. 2002; 26(1):62–68. [PubMed: 11801905]
10. Tortorella P, Rocca MA, et al. MRI quantification of gray and white matter damage in patients with early-onset multiple sclerosis. J Neurol. 2006; 253(7):903–907. [PubMed: 16511645]
11. Allen IV, McKeown SR. A histological, histochemical and biochemical study of the macroscopically normal white matter in multiple sclerosis. J Neurol Sci. 1979; 41:81–91. [PubMed: 438845]
12. Trapp BD, Peterson J, Ransohoff RM, Rudick R, Mork S, Bo L. Axonal transection in the lesions of multiple sclerosis. N Engl J Med. 1998; 338:278–85. [PubMed: 9445407]
13. Kutzelnigg A, Lucchinetti CF, Stadelmann C, Bruck W, Rauschka H, Bergmann M, et al. Cortical demyelination and diffuse white matter injury in multiple sclerosis. Brain. 2005; 128:2705–12. [PubMed: 16230320]
14. Peterson JW, Bo L, Mork S, Chang A, Trapp BD. Transected neurites, apoptotic neurons, and reduced inflammation in cortical multiple sclerosis lesions. Ann Neurol. 2001; 50:389–400. [PubMed: 11558796]
15. Van der Flier WM, van den Heuvel DM, Weverling-Rijnsburger AW, et al. Magnetization transfer imaging in normal aging, mild cognitive impairment, and Alzheimer's disease. Ann Neurol. 2002; 52(1):62–67. [PubMed: 12112048]
16. Ridha BH, Tozer DJ, Symms MR, et al. Quantitative magnetization transfer imaging in Alzheimer disease. Radiology. 2007; 244(3):832–837. [PubMed: 17709831]
17. Hanyu H, Asano T, Sakurai H, et al. Magnetization transfer measurements of the hippocampus in the early diagnosis of Alzheimer's disease. J Neurol Sci. 2001; 188(1–2):79–84. [PubMed: 11489289]

18. Ginestroni A, Battaglini M, Della Nave R, et al. Early structural changes in individuals at risk of familial Alzheimer's disease: a volumetry and magnetization transfer MR imaging study. J Neurol. 2009; 256(6):925–932. [PubMed: 19252791]
19. van Es AC, van der Flier WM, Admiraal-Behloul F, et al. Magnetization transfer imaging of gray and white matter in mild cognitive impairment and Alzheimer's disease. Neurobiol Aging. 2006; 27(12):1757–1762. [PubMed: 16290268]
20. Seppi K, Schocke MF, Esterhammer R, et al. Diffusion-weighted imaging discriminates progressive supranuclear palsy from PD, but not from the parkinson variant of multiple system atrophy. Neurology. 2003; 60(6):922–927. [PubMed: 12654954]
21. Nicoletti G, Lodi R, Condino F, et al. Apparent diffusion coefficient measurements of the middle cerebellar peduncle differentiate the Parkinson variant of MSA from Parkinson's disease and progressive supranuclear palsy. Brain. 2006; 129(Pt 10):2679–2687. [PubMed: 16815875]
22. Anik Y, Iseri P, Demirci A, et al. Magnetization transfer ratio in early period of Parkinson disease. Acad Radiol. 2007; 14(2):189–192. [PubMed: 17236991]
23. van Buchem MA, McGowan JC, Kolson DL, et al. Quantitative volumetric magnetization transfer analysis in multiple sclerosis: estimation of macroscopic and microscopic disease burden. Magn Reson Med. 1996; 36(4):632–636. [PubMed: 8892218]
24. Filippi M. Magnetization transfer imaging to monitor the evolution of multiple sclerosis. Ital J Neurol Sci. 1999; 20(5 Suppl):S232–240. [PubMed: 10662954]
25. Grossman RI. Application of magnetization transfer imaging to multiple sclerosis. Neurology. 1999; 53(5 Suppl 3):S8–11. [PubMed: 10496204]
26. Rovaris M, Bozzali M, Rodegher M, et al. Brain MRI correlates of magnetization transfer imaging metrics in patients with multiple sclerosis. J Neurol Sci. 1999; 166(1):58–63. [PubMed: 10465501]
27. Barkhof F, Calabresi PA, Miller DH, Reingold SC. Imaging outcomes for neuroprotection and repair in multiple sclerosis trials. Nat Rev Neurol. 2009; 5:256–266. [PubMed: 19488083]
28. Ge Y, Kolson DL, Babb JS, et al. Whole brain imaging of HIV-infected patients: quantitative analysis of magnetization transfer ratio histogram and fractional brain volume. AJNR. 2003; 24(1): 82–87. [PubMed: 12533331]
29. Wu Y, Storey P, Carrillo A, et al. Whole brain and localized magnetization transfer measurements are associated with cognitive impairment in patients infected with human immunodeficiency virus. AJNR. 2008; 29(1):140–145. [PubMed: 17928382]
30. Kubicki M, Park H, Westin CF, et al. DTI and MTR abnormalities in schizophrenia: analysis of white matter integrity. Neuroimage. 2005; 26(4):1109–1118. [PubMed: 15878290]
31. Dousset V, Grossman RI, Ramer KN, et al. Experimental allergic encephalomyelitis and multiple sclerosis: lesion characterization with magnetization transfer imaging. Radiology. 1992; 182(2): 483–491. [PubMed: 1732968]
32. Filippi M, Campi A, Dousset V, et al. A magnetization transfer imaging study of normal-appearing white matter in multiple sclerosis. Neurology. 1995; 45(3 Pt 1):478–482. [PubMed: 7898700]
33. Wu, Y.; Du, HK.; Zou, KH., et al. Reliability and reproducibility of high magnetization Transfer Imaging on 3T. International Society of Magnetic Resonance in Medicine; 2008; Toronto, Canada.
34. Berry I, Barker GJ, Barkhof F, et al. A multicenter measurement of magnetization transfer ratio in normal white matter. J Magn Reson Imaging. 1999; 9(3):441–446. [PubMed: 10194715]
35. Tofts PS, Steens SCA, Cercignani M, et al. Sources of variation in multi-centre brain MTR histogram studies: body-coil transmission eliminates inter-centre differences. Magn Reson Mater Phy. 2006; 19:209–222.
36. Cercignani M, Symms MR, Ron M, Barker GJ. 3D MTR measurement: from 1.5 T to 3.0 T. Neuroimage. 2006; 31(1):181–186. [PubMed: 16413794]
37. Smith SA, Reich DS, Jones CK, et al. Quantitative characterization of the corticospinal tract at 3T. AJNR. 2006; 27(10):2168–2178. [PubMed: 17110689]
38. Helms G, Dathe H, Kallenberg K, Dechent P. High-resolution maps of magnetization transfer with inherent correction for RF inhomogeneity and T1 relaxation obtained from 3D FLASH MRI. Magn Reson Med. 2008; 60(6):1396–1407. [PubMed: 19025906]

39. Helms G, Dathe H, Dechent P. Modeling the influence of TR and excitation flip angle on the magnetization transfer ratio (MTR) in human brain obtained from 3D spoiled gradient echo MRI. Magn Reson Med. 2010; 64(1):177–185. [PubMed: 20572139]
40. Wu Y, Warfield SK, Tan IL, et al. Automated segmentation of multiple sclerosis lesion subtypes with multichannel MRI. Neuroimage. 2006; 32(3):1205–1215. [PubMed: 16797188]
41. Wu, Y.; Du, H.; Malone, F., et al. Automated volume of interest evaluation for sequence development. International Society for Magnetic Resonance Imaging in Medicine; 2009; Honolulu, Hawaii.
42. Jack CR Jr, Bernstein MA, Fox NC, et al. The Alzheimer's Disease Neuroimaging Initiative (ADNI): MRI methods. J Magn Reson Imaging. 2008; 27(4):685–691. [PubMed: 18302232]
43. Wu, Y.; O'Brien, C.; Glielmi, C.; Du, H.; Edelman, RR.; Ragin, A. High Resolution Magnetization Transfer Imaging at 3T vs. 1.5T. International Society of Magnetic Resonance Imaging Conference; 2010; Stockholm, Sweden.
44. Smith SM, Jenkinson M, Woolrich MW, et al. Selective gray matter damage in neuropsychiatric lupus. Arthritis Rheum. 2004; 50(9):2877–2881. [PubMed: 15457455]
45. Fischl B, Salat DH, Busa E, et al. Whole brain segmentation: automated labeling of neuroanatomical structures in the human brain. Neuron. 2002; 33(3):341–355. [PubMed: 11832223]
46. Wu Y, Storey P, Carrillo A, Saglamer C, Cohen BA, Epstein LG, Edelman RR, Ragin AB. Whole brain and localized magnetization transfer measurements are associated with cognitive impairment in patients infected with human immunodeficiency virus. AJNR Am J Neuroradiol. 2008 Jan; 29(1):140–5. Epub 2007 Oct 10. [PubMed: 17928382]
47. Wu Y, Storey P, Cohen BA, Epstein LG, Edelman RR, Ragin AB. Diffusion alterations in corpus callosum of patients with HIV. AJNR Am J Neuroradiol. 2006 Mar; 27(3):656–60. [PubMed: 16552012]
48. Ramani A, Jensen JH, Helpern JA. Quantitative MR imaging in Alzheimer disease. Radiology. 2006; 241(1):26–44. [PubMed: 16990669]
49. Bland JM, Altman DG. Statistical methods for assessing agreement between two methods of clinical measurement. Lancet. 1986; i:307–310. [PubMed: 2868172]
50. Haynes, BI.; Dowell, NG.; Tofts, PS. Measuring scan-rescan reliability in quantitative brain imaging reveals instability in an apparently healthy imager and improves statistical power in a clinical study. International Society of Magnetic Resonance Imaging Conference; 2010; Stockholm, Sweden.
51. Zou KH, Du H, Sidharthan S, et al. Statistical evaluations of the reproducibility and reliability of 3-tesla high resolution magnetization transfer brain images: a pilot study on healthy subjects. Int J Biomed Imaging. 2010:618747. [PubMed: 20169129]
52. Shrout, PE.; Fleiss, J. Intraclass correlations: Uses in Assessor Rate Reliability. 1979.
53. Tofts, PS. QA: Quality assurance, accuracy, precision and phantoms (chapter 3). In: Tofts, Paul, editor. Quantitative MRI of the brain: measuring changes caused by disease. Chichester: John Wiley; 2003. p. 55-81.
54. McLaughlin, SC.; Aitchison, TC.; Macfarlane, PW. The Value of COV in Assessing Repeat Variation in ECG Measurement. 1998.
55. Smith SA, Jones CK, Glifford A, et al. Reproducibility of tract-specific magnetization transfer and diffusion tensor imaging in the cervical spinal cord at 3 tesla. NMR Biomed. 2010; 23(2):207–217. [PubMed: 19924726]
56. Martirosian P, Boss A, Deimling M, et al. Systematic variation of off-resonance prepulses for clinical magnetization transfer contrast imaging at 0.2, 1.5, and 3.0 tesla. Invest Radiol. 2008; 43(1):16–26. [PubMed: 18097273]
57. Hanyu H, Asano T, Iwamoto T, et al. Magnetization transfer measurements of the hippocampus in patients with Alzheimer's disease, vascular dementia, and other types of dementia. AJNR. 2000; 21(7):1235–1242. [PubMed: 10954274]
58. Kabani NJ, Sled JG, Chertkow H. Magnetization transfer ratio in mild cognitive impairment and dementia of Alzheimer's type. Neuroimage. 2002; 15(3):604–610. [PubMed: 11848703]

59. Gringel T, Schulz-Schaeffer W, Elolf E, et al. Optimized high-resolution mapping of magnetization transfer (MT) at 3 Tesla for direct visualization of substructures of the human thalamus in clinically feasible measurement time. J Magn Reson Imaging. 2009; 29(6):1285–1292. [PubMed: 19472385]
60. Filippi M, Campi A, Dousset V, et al. A magnetization transfer imaging study of normal-appearing white matter in multiple sclerosis. Neurology. 1995; 45(3 Pt 1):478–82. [PubMed: 7898700]
61. Silver NC, Barker GJ, MacManus DG, et al. Magnetisation transfer ratio of normal brain white matter: a normative database spanning four decades of life. J Neurol Neurosurg Psychiatry. 1997; 62(3):223–228. [PubMed: 9069474]
62. Ge Y, Grossman RI, Babb JS, et al. Age-related total gray matter and white matter changes in normal adult brain. Part II: quantitative magnetization transfer ratio histogram analysis. AJNR Am J Neuroradiol. 2002; 23(8):1334–1341. [PubMed: 12223374]
63. Davies GR, Altmann DR, Hadjiprocopis A, et al. Increasing normal-appearing grey and white matter magnetisation transfer ratio abnormality in early relapsing-remitting multiple sclerosis. J Neurol. 2005; 252(9):1037–1044. [PubMed: 15834645]
64. Khaleeli Z, Sastre-Garriga J, Ciccarelli O, et al. Magnetisation transfer ratio in the normal appearing white matter predicts progression of disability over 1 year in early primary progressive multiple sclerosis. J Neurol Neurosurg Psychiatry. 2007; 78(10):1076–1082. [PubMed: 17287235]
65. Vrenken H, Pouwels PJ, Ropele S, et al. Magnetization transfer ratio measurement in multiple sclerosis normal-appearing brain tissue: limited differences with controls but relationships with clinical and MR measures of disease. Mult Scler. 2007; 13(6):708–716. [PubMed: 17613597]
66. Bellmann-Strobl J, Stiepani H, Wuerfel J, et al. MR spectroscopy (MRS) and magnetisation transfer imaging (MTI), lesion load and clinical scores in early relapsing remitting multiple sclerosis: a combined cross-sectional and longitudinal study. Eur Radiol. 2009; 19(8):2066–2074. [PubMed: 19308417]

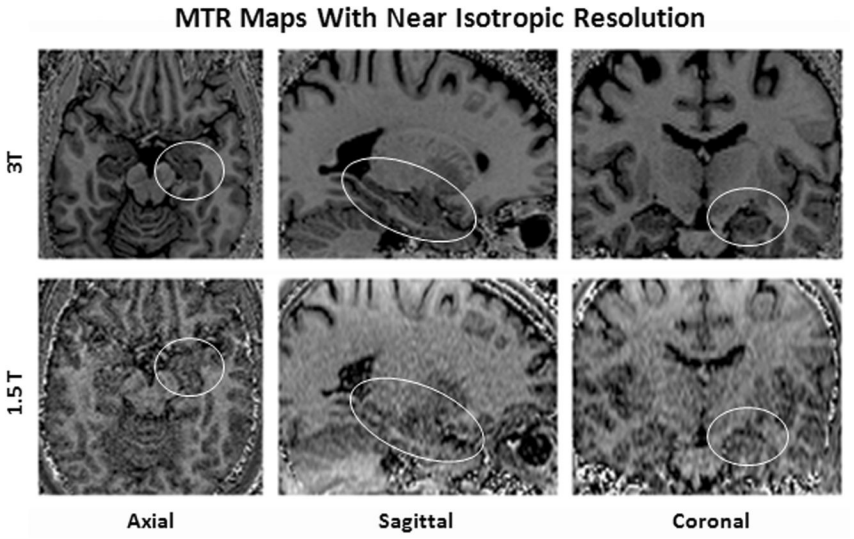

Fig. 1.

High resolution MTR maps at 1.5T and 3T. Note the marked differences in conspicuity of the hippocampal areas (circled) and the overall higher image quality at 3T axial initial scan orientation as well as reformatted sagittal and coronal planes (Imaging resolution: 1.0 × 1.0 × 1.2 mm^3).

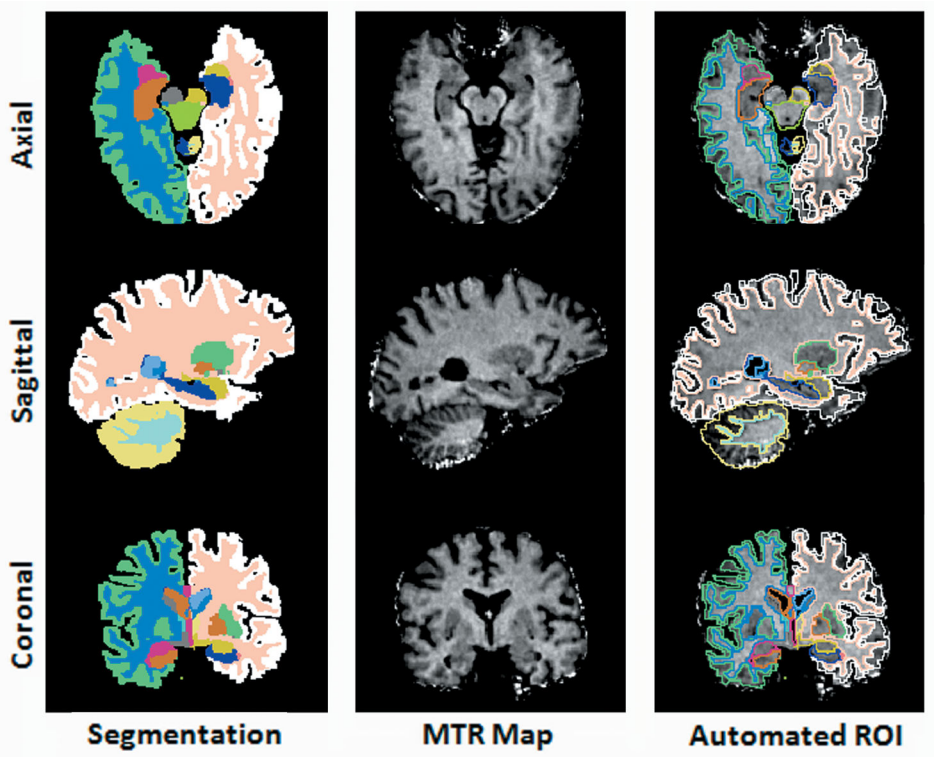

Fig. 2.

The first column: the representation of automated segmentation in 3 spatial orientations. The second column: the re-sliced MTR maps were spatially aligned with segmentation maps possessing isotropic voxel resolution identical to that of the segmentation maps. The third column: brain structures labeled in the segmentation maps (column 1) were used to automatically delineate brain volume of interest and extract regional MTR measurements. Segmentation color code: Right Hippocampus: orange, Left Hippocampus: dark blue, Right Amygdala: magenta, Left Amygdala: yellow, Right Putamen: blue, Left Putamen: green, Right Cortical Gray Matter: light green, Left Cortical Gray Matter: white, Right Cortical White Matter: sky blue, Left Cortical White Matter: peach.

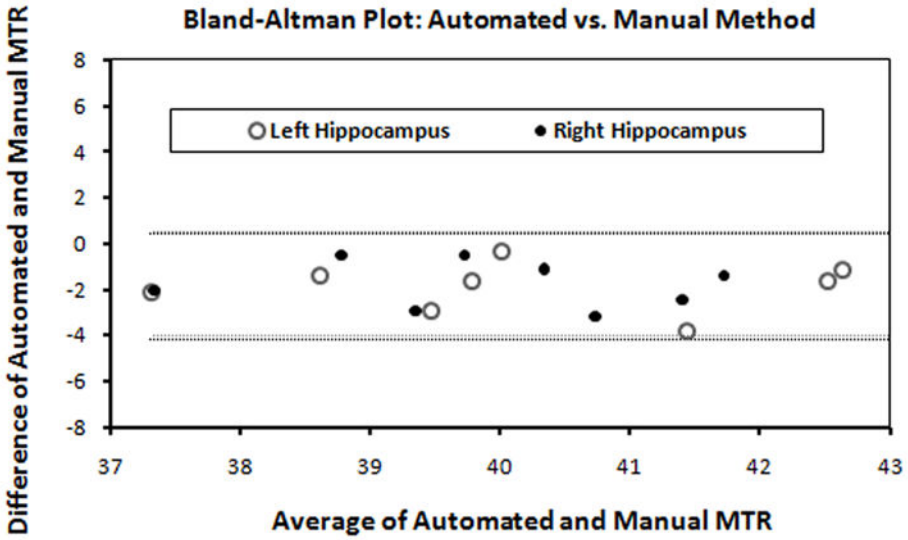

Fig. 3.

The Bland-Altman plot shows MTR measurements derived from automated and manual methods demonstrating excellent agreement (hippocampus data shown).

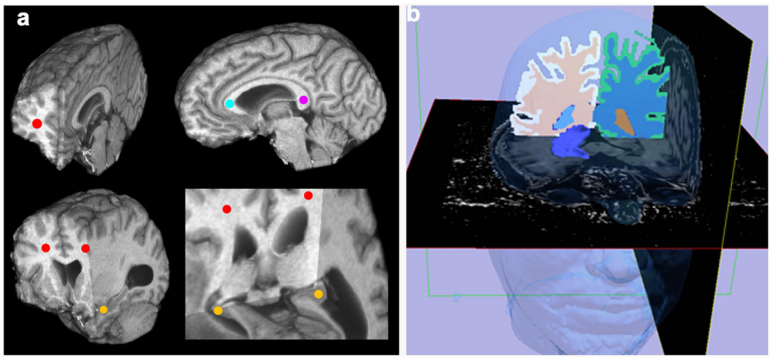

Fig. 4.

Examples of the manual ROI method and the automated VOI method of MTR measurement. 4a: 3D high resolution MTR maps were transected at multiple planes to expose the manual ROI placements represented by the colored dots at various brain regions: left and right white matter (red), genu (aqua), splenium (magenta) and hippocampus (yellow). 4b: A 3D model of right hippocampus was generated and superimposed to the MTR map to illustrate the automated VOI measurement extraction. The high resolution MTR maps were displayed for Axial and Sagittal planes and the automated segmentation masks were displayed for the Coronal plane. The left hippocampus can be visualized at the gray scale MTR map of the Axial plane demonstrating anatomical detail. The 3D face (above) was reconstructed as a spatial orientation reference. Color code: Hippocampus: Purple, Right white matter: Peach, Left white matter: Blue, Face: Blue Transparent.

Table 1

Comparison between Automated and Manual Methods

	Automated Method					Manual Method				
	Mean MTR S1 (pu)	Mean MTR S2 (pu)	ICC	CV (%)	ISD (pu)	Mean MTR S1 (pu)	Mean MTR S2 (pu)	ICC	CV (%)	ISD (pu)
Gray Matter Regions										
Left amyg	41.94	41.41	0.92	2.64	1.10	42.21	42.02	0.87	3.40	1.43
Right amyg	42.06	41.63	0.90	2.29	0.96	42.04	42.67	0.85	2.83	1.20
Left cau	40.31	39.65	0.92	2.18	0.87	40.80	39.87	0.93	2.21	0.89
Right cau	39.82	39.05	0.93	2.13	0.84	40.12	39.99	0.94	2.10	0.84
Left put	41.22	40.82	0.93	2.05	0.84	41.75	41.86	0.86	2.94	1.23
Right put	41.02	40.71	0.96	1.52	0.62	42.03	41.90	0.95	1.57	0.66
Left thal	45.61	44.94	0.95	1.50	0.68	45.47	45.51	0.93	1.80	0.82
Right thal	45.97	45.09	0.93	1.63	0.74	45.60	46.25	0.96	1.39	0.64
Left hipp	39.88	40.10	0.92	2.33	0.93	41.00	41.93	0.76	4.03	1.67
Right hipp	40.01	39.92	0.94	1.83	0.73	41.05	40.68	0.84	3.01	1.23
White Matter Regions										
Left WM	49.47	49.23	0.84	1.56	0.77	49.28	49.23	0.88	1.44	0.71
Right WM	49.93	49.54	0.89	1.29	0.64	49.30	48.82	0.85	1.83	0.9
Genu	50.59	49.97	0.77	1.83	0.92	52.21	52.13	0.89	1.30	0.68
Splen	51.31	50.93	0.88	1.47	0.75	52.62	51.81	0.80	2.13	1.11

S1 and S2- Time-point 1 and Time-point 2, ISD-Instrumental Standard Deviation, CV-Coefficient of Variation, ICC- Intra Class Correlation Coefficient, L-Left, R-Right, Amyg-Amygdala, Caud-Caudate, Puta-Putamen, Thal-Thalamus, Hipp-Hippocampus, WM-White Matter, SN-Substantia Nigra, Genu-Genu, Splen-Splenium.

Table 2

Analysis Operator Variation of Manual MTR Measurements

	ROI	Amyg		Caud		Puta		Thal		Hipp		WM		Genu	Splen
		L	R	L	R	L	R	L	R	L	R	L	R		
CV %	Intra-rater	5.34	3.83	2.52	3.69	3.47	2.72	2.67	2.60	5.90	3.54	2.37	2.58	1.40	2.64
	Inter-rater	2.57	2.65	2.28	2.01	2.30	2.28	3.70	3.62	3.64	3.81	5.50	4.93	4.74	5.11

CV-Coefficient of Variation, L-Left, R-Right, Amyg-Amygdala, Caud-Caudate, Puta-Putamen, Thal-Thalamus, Hipp-Hippocampus, WM-White Matter, Genu-Genu, Splen-Splenium

Table 3

Instrumental variation in a phantom

Scan	5.0%	2.5%	2.0%	1.5%	1.0%	0.5%
1	-	-	-	-	-	-
2	−0.96%	0.02%	3.19%	5.53%	−1.88%	−1.98%
3	2.91%	−0.63%	−0.97%	−1.10%	1.78%	1.13%
4	−1.67%	0.72%	−4.67%	0.57%	−0.45%	−1.78%
5	1.66%	−2.60%	4.36%	−2.54%	−2.08%	1.71%
6	−3.73%	0.92%	−2.67%	0.23%	−0.30%	0.47%
7	2.12%	−2.60%	−1.61%	1.53%	−1.13%	−7.95%
8	1.34%	6.17%	5.49%	4.32%	3.86%	11.12%
9	−1.23%	−2.15%	−1.37%	−5.13%	−0.76%	−1.11%
10	0.87%	0.45%	2.98%	−1.29%	0.23%	−2.42%
11	−1.09%	−1.55%	−1.95%	4.65%	2.36%	1.12%
12	0.06%	−2.18%	−4.41%	−5.24%	−3.79%	−3.43%
13	0.30%	4.92%	7.41%	−0.04%	3.26%	4.55%
14	0.05%	−2.03%	−2.30%	5.41%	−0.58%	−2.67%
15	−1.31%	−2.44%	−2.57%	−4.45%	−1.68%	−6.86%
16	0.48%	−0.03%	0.23%	2.17%	−1.75%	9.51%
SD	1.70%	2.66%	3.71%	3.67%	2.14%	5.23%